Synthesis, Crystal Structure, and Enthalpies of Formation of Churchite-type REPO 4 ×2H 2 O (RE = Gd to Lu) Materials

Tamilarasan Subramani, Mohamed Ruwaid Rafiuddin, Anna Shelyug, Sergey V. Ushakov, Adel Mesbah, Nicolas Clavier, Danwen Qin, Stephanie Szenknect, Erik Elkaïm, Nicolas Dacheux, et al.

Synthesis, Crystal Structure and Enthalpies of Formation of Churchite-type $REPO_4 \cdot 2\ H_2O$ (RE = Gd to Lu) Materials.

Tamilarasan Subramani,[†] Mohamed Ruwaid Rafiuddin,[‡] Anna Shelyug,[†] Sergey Ushakov,[†] Adel Mesbah,[‡,] Nicolas Clavier,[‡] Danwen Qin,[‡] Stephanie Szenknect,[‡] Erik Elkaim,[§], Nicolas Dacheux,[‡] Alexandra Navrotsky[†,*]*

[†]Peter A. Rock Thermochemistry Laboratory and NEAT ORU, University of California Davis, Davis CA 95616 USA

[‡]ICSM, CEA, CNRS, ENSCM, Univ Montpellier, Site de Marcoule, Bat 426, 30207 Bagnols Sur Ceze, France

§ Synchrotron SOLEIL, L'Orme des Merisiers, Saint-Aubin, BP 48, 91192 Gif Sur Yvette, France

Abstract

Monazite- ($REPO_4$; RE = La to Gd) and xenotime- ($REPO_4$; RE = Dy to Lu & Y) type materials have been proposed as host matrices for the immobilization of actinides. Aqueous alteration of monazite and xenotime minerals could result in the formation of rhabdophane ($REPO_4 \cdot 0.667\ H_2O$; RE = La to Dy) and churchite ($REPO_4 \cdot 2\ H_2O$; RE = Gd to Lu & Y) phases, respectively. Among these structure types, the structure and properties of churchite materials are not well understood and this study aims to bridge this gap by providing a comprehensive insight into the structure and thermochemical properties of churchite materials. Churchite materials ($REPO_4 \cdot 2\ H_2O$; RE = Gd to Lu) were synthesized by a low temperature precipitation route and their crystal structures were determined by powder X-ray diffraction (XRD). Examination of the powder XRD data has shown that the churchite materials crystallize in the monoclinic crystal system (space group: *C*2/c). The enthalpies of formation ($\Delta H°_{f,ox}$) of churchite-type $REPO_4 \cdot 2\ H_2O$ (RE = Gd to Yb) determined by high temperature oxide melt solution calorimetry are more negative than their anhydrous counterparts (i.e., xenotime structure) and indicates that the formation of churchite is more exothermic than the xenotime phase. However, the churchite materials are likely to have a more negative entropy of formation ($\Delta S°_{f,ox}$) due to the presence of water molecules, resulting in a less negative Gibbs free energy of formation ($\Delta G°_{f,ox}$) than the xenotime structure. Therefore, churchite materials are expected to be stable at lower temperatures. For the unique case of $GdPO_4$ and $GdPO_4 \cdot n\ H_2O$ materials which could adopt all the above discussed structure types, the $\Delta G°_{f,ox}$ of monazite from oxides was observed to be more negative than those of xenotime, rhabdophane and churchite thereby suggesting the following order of stability: Gd-churchite < Gd-rhabdophane < Gd-xenotime < Gd-monazite.

Introduction

Rare earth (RE) phosphate materials have been the subject of numerous investigations particularly owing to their potential use as a host matrix for the storage of high level wastes (HLW) arising from the reprocessing of spent nuclear fuel and dismantling of nuclear weapons.[1-6] RE phosphates are both compositionally and structurally diverse and occur in nature as monazite ($REPO_4$; RE = La to Gd), xenotime ($REPO_4$; RE = Gd to Lu & Y), rhabdophane ($REPO_4 \cdot n\ H_2O$; RE = La to Dy; $0 \leq n \leq 0.667$), and churchite ($REPO_4 \cdot 2\ H_2O$; RE = Gd to Lu and Y).[7-10] Among these minerals, monazite and xenotime minerals contain the highest weight percent of rare earth elements. In addition, they also contain a large amount of U and Th thereby making these minerals radioactive. Even though, these minerals have been exposed to radiation events over geological timescales,[11-14] it should be noted that the monazite mineral, in particular, is never completely found in the metamict state (i.e. amorphization due to radiation damages). Radiation studies on synthetic and natural monazite samples have shown that the monazite samples experience structural damage upon heavy-ion (e.g., Au ions) irradiation and can also recover completely from the structural damage upon annealing the irradiated samples at low temperatures or via light-ion (e.g., He ions) irradiation of the damaged samples.[15-20] Nevertheless, apart from a few radiation studies on synthetic xenotime samples, the structural response of xenotime minerals to radiation is not well documented.[17] In terms of chemical durability, both monazite and xenotime minerals are reported to be chemically durable in aqueous environments.[21-25] Such mineralogical evidence suggests that the synthetic analogues of monazite and xenotime minerals are promising matrices for the immobilization of high level nuclear waste (HLW).[2,26] Moreover, hydrated RE phosphates, namely rhabdophane is found to form on the surface of monazite minerals during the aqueous alteration and thus they efficiently

stop or delay the release of actinides to the environment.[8,27,28] Besides applications as nuclear waste forms, the rare-earth phosphates also have wide ranging applications in photonics, as catalysts, as proton conductors, and in biolabeling.[29-33]

Rare earth phosphates can adopt the monazite-, xenotime-, rhabdophane-, and churchite-type structures depending on the ionic radius of the RE ions as well as the conditions of the synthesis. Using specific synthetic methods and conditions, it is possible to obtain all the above-mentioned crystal structures for the following rare-earths: Gd, Tb, and Dy. Anhydrous RE phosphates adopting the monazite- ($REPO_4$; RE = La to Gd) and xenotime structures ($REPO_4$; RE' = Tb to Lu and Y) crystallize in the monoclinic (space group: $P2_1/n$) and tetragonal (space group: $I4_1/amd$) crystal systems, respectively.[7] Hydrated RE phosphates adopting the rhabdophane structure ($REPO_4 \cdot n\ H_2O$; RE = La to Dy; $0 \leq n \leq 0.667$) crystallize in the monoclinic crystal system (space group: $C2$) while the corresponding anhydrous form of rhabdophane materials ($REPO_4$; RE = La to Dy) adopt the trigonal structure (space group: $P3_121$).[8,34] Detailed descriptions of the crystal structures of monazite, xenotime, and rhabdophane can be found elsewhere.[7,8,34] While the structures of monazite, xenotime, and rhabdophane materials have been studied in much detail, the churchite ($REPO_4 \cdot 2\ H_2O$; RE = Gd to Lu and Y) materials have been less explored. To the best of our knowledge, there has been only two structural studies reported on churchite-type materials.[9,10] Those were carried out on synthetic ($YPO_4 \cdot 2\ H_2O$) and natural churchite ($Y_{1-x}(Gd,Dy,Er)_xPO_4 \cdot 2\ H_2O$) samples.[9,10] Both these studies have shown that the churchite materials adopt the gypsum structure ($CaSO_4 \cdot 2\ H_2O$) and crystallize in the monoclinic system (space group: $C2/c$).[9,10] With the exception of $GdPO_4 \cdot 2\ H_2O$, the synthesis and crystal structure of other members of the churchite group materials ($REPO_4 \cdot 2\ H_2O$; RE = Tb to Lu) have not been reported yet.[35] While the

thermodynamic properties of anhydrous RE phosphates adopting the monazite and xenotime structures are fairly well understood, those of hydrous RE phosphates adopting the churchite structures are limited.[36-38]

This study reports the synthesis, structure, and thermochemical properties of the churchite materials $REPO_4 \cdot 2\ H_2O$ (RE = Gd to Lu). Members of the churchite series were prepared using a precipitation route and their crystal structures were determined using laboratory and synchrotron powder X-ray diffraction (XRD). Thermal analysis was conducted using differential scanning calorimetry (DSC) and thermogravimetric analysis (TGA). The enthalpies of formation of the entire churchite series were determined by high temperature oxide melt solution calorimetry. The systematics of structure and thermodynamic stability are discussed. To the best of our knowledge, this represents the first study to carry out the synthesis and the structural and thermochemical characterization of all members of the churchite ($REPO_4 \cdot 2\ H_2O$; RE = Gd to Lu) series.

Experimental methods

Synthesis

The synthesis of $REPO_4 \cdot 2\ H_2O$ materials was performed using the following starting materials: $GdCl_3 \cdot 6\ H_2O$ (Sigma Aldrich; 99 %), $TbCl_3 \cdot 6\ H_2O$ (Sigma Aldrich; 99.9%), $DyCl_3 \cdot 6\ H_2O$ (Sigma Aldrich; 99.99 %), $HoCl_3$ (Sigma Aldrich, 99.9 %), $ErCl_3 \cdot n\ H_2O$ (Sigma Aldrich; 99.9 %), $TmCl_3$ (Sigma Aldrich; 99.9 %), $YbCl_3$ (Sigma Aldrich; 99.9 %), $LuCl_3$ (Sigma Aldrich; 99.9%), H_3PO_4 (85% Normapur), and HCl (37 % Carbo Erba). The hygroscopic nature of the lanthanide chloride salts prevents the accurate weighing of these powders. For this reason, these salts were dissolved in 1M HCl to prepare solutions whose

lanthanide concentration varied between 0.5 and 1M. The final concentrations of the dissolved lanthanides were further determined by ICP-AES.

Pure $REPO_4$ 2 H_2O (RE = Gd, Tb, Dy, Ho, Er, Tm, Yb, Lu) materials were synthesized by mixing lanthanide chloride solutions and H_3PO_4 (5 M) with 3 mol. % phosphate excess. Then, each mixture was transferred in a glass container (100 mL) and left aside in a refrigerator at 4°C for two years. Afterwards, the resulting powder was washed twice with water, and once with ethanol, separated from the solution by centrifugation and then finally dried at room temperature in air. In order to determine the thermodynamic stability of monazite-, xenotime-, rhabdophane-, and churchite type structures for a given RE element, Gd-phosphates adopting these structure-types were also synthesized.

Powder X-Ray Diffraction (PXRD)

Synchrotron powder diffraction pattern of selected compounds $REPO_4 \cdot 2\ H_2O$ (Ln = Gd, Dy and Er) were collected from the beamline "Cristal" at Synchrotron Soleil, France in high angular resolution mode using the two-circle diffractometer equipped with twenty one Si(111) crystals rear analyzers. Scans were recorded at room temperature with the powder inside a glass capillary (diameter 0.3 mm) mounted on a spinner to improve particle statistics. A wavelength of 0.58403 Å was selected and calibrated using LaB_6 standard NIST powder. With this setup, a single scan was collected up to $2\theta = 60$ ° in about two hours. In order to avoid the degradation of the powder under irradiation, the capillary was shifted to a fresh zone every 15 minutes.

All the as-synthesized powders were also analyzed using laboratory PXRD and the data were collected in reflection geometry mode using a Bruker D8-Advance diffractometer (LynxEye detector) employed with Cu $K\alpha_{1,2}$ radiation ($\lambda = 1.5418$ Å) source. Data were recorded at room temperature from 5° to 120° using a step size $\Delta(2\theta) = 0.0167$ ° and a total counting time

of about 2 hours per sample. All the collected powder patterns (see Figure 1) have been refined by the Rietveld method using the Fullprof program suite.[39] The refinement of the crystal structure was performed using the Thompson-Cox-Hastings pseudo-Voigt function convoluted with axial divergence asymmetry function.[40] The instrumental function was extracted from LaB_6 mentioned above. During the refinement, in addition of the usual parameters the broadening effect was simulated by using an anisotropic size effect in agreement with the Laue group.

Scanning Electron Microscopy

SEM images were collected from powders of churchite-type $ErPO_4 \cdot 2\ H_2O$ material using a Tescan Vega 3 electronic microscope. Powders of as-synthesized $ErPO_4 \cdot 2\ H_2O$ were mounted on a double-sided carbon tape and no metallization was performed prior to image collection. The images were collected in secondary electron mode from various locations of the sample under high vacuum conditions and using an accelerating voltage of 30 kV.

Thermal analysis

Differential scanning calorimetry (DSC) and thermogravimetric analysis (TGA) was performed using a Netzsch 449 TG/DSC instrument to determine the water content in the as-synthesized churchite samples. The instrument was calibrated using sapphire heat capacity measurement. 10 - 15 mg of sample powder was heated in a Pt crucible under argon atmosphere from room temperature to 1000 °C at 10 °C/min.

High temperature oxide melt solution calorimetry

High temperature oxide melt solution calorimetry for all the samples was performed employing a custom built Tian-Calvet twin calorimeter.[41-44] About 5 mg of pelletized samples were dropped into molten sodium molybdate ($3\ Na_2O \cdot 4\ MoO_3$) solvent at 700 °C. The calorimetry glassware was flushed by argon gas at a flow rate of 30 mL/min and the solvent was

bubbled with the same gas at a flow rate of 5 mL/min throughout each measurement. At least 8-10 experiments were done per sample and the results report are average values with error being two standard deviations of the mean. The calorimeter was calibrated using the heat content of 5 mg pellets of α-Al_2O_3. The details of the calorimeter and procedures have been described previously.[41-44]

Results and discussion

Synthesis and Microstructure

According to the literature, the churchite-type $REPO_4 \cdot 2\ H_2O$ materials were synthesized via wet-chemistry methods at temperatures between room temperature and 40 °C and using excess phosphoric acid (molar ratio P/RE = 20). Initial attempts to synthesize phase-pure churchite-type materials by following the reported synthetic protocols resulted in a mixture of churchite (major), rhabdophane (minor), and xenotime (minor) phases.[9] For Gd, Tb and Dy elements, rhabdophane was observed as the secondary phase and for the heavier rare-earth elements ranging from Ho to Lu, xenotime was observed as the secondary phase. Therefore, several experiments were performed by varying the PO_4/RE molar ratio (with RE= Gd, Er) and the temperature of synthesis. Based on our investigations into the syntheses, it was found that the decrease of temperature had a direct influence on the phase purity of the churchite. In this way, the temperature of the synthesis was decreased to 4 °C and pure churchite-type materials were synthesized.

The microstructure of the churchite materials was determined by collecting the SEM images from one of the members of the churchite series ($ErPO_4 \cdot 2\ H_2O$). The SEM images of $ErPO_4 \cdot 2\ H_2O$ obtained at different magnifications from two different locations are presented in Figure 2. It can be observed in Figure 2, that the churchite materials exhibit a rod-like morphology and is similar to the morphology exhibited by gypsum ($CaSO_4 \cdot 2\ H_2O$) materials.

Structure

The crystal structure of churchite materials was determined by performing a Rietveld refinement of the synchrotron powder XRD pattern of $ErPO_4 \cdot 2\ H_2O$ material using the monoclinic structural model ($YPO_4 \cdot 2\ H_2O$; Space group: *C*2/c) reported by Ivaskevich et al.[9] As is observed in Figure 1, the calculated XRD pattern matches well with the experimental powder XRD pattern which confirms that the as-synthesized churchite-type materials adopt the monoclinic system. The lattice constants and the refined structural parameters of $ErPO_4 \cdot 2\ H_2O$ material are presented in Table 1. The synchrotron powder XRD patterns of other members of the churchite series ($REPO_4 \cdot 2\ H_2O$; RE = Gd, Dy) were also refined using the monoclinic structural model (See Figure S1 in the Supporting Information and Table 1). It should be noted that the as-synthesized $GdPO_4 \cdot 2\ H_2O$ material was found to crystallize in both churchite-type (major) and rhabdophane-type (minor) structures (Figure S1a). The laboratory powder XRD patterns were also collected from $REPO_4 \cdot 2\ H_2O$ (RE = Gd to Lu) materials and are shown in Figure 3. It can be observed from this figure that on moving from Gd to Lu, the XRD peaks shifted toward higher 2θ, which indicates the contraction of the unit cell dimension (Figure 3 and Table 3). This observation is consistent with the decreasing ionic radius of RE ion on moving from Gd to Lu. Similarly, the unit cell volumes of the $REPO_4 \cdot 2\ H_2O$ materials were found to decrease with decreasing ionic radii (Table 3 and Figure 4).

The obtained churchite phases crystallize in the gypsum structure type ($CaSO_4 \cdot 2\ H_2O$) in the monoclinic system in the C2/c space group with four formula units per cell. The asymmetric units contain one RE atom (*2*, symmetry site), one P atom (*2*, symmetry site) and three oxygen atoms located in a general position (*1*, symmetry site). The crystal structure of representative churchite type $ErPO_4 \cdot 2\ H_2O$ material is presented in Figure 5.

The Er atom in the $ErPO_4 \cdot 2\ H_2O$ is coordinated to eight oxygen atoms. Six of them are provided by the phosphate anions whereas the remaining two oxygen atoms are provided by water molecules. The resulting ErO_8 polyhedron adopts a highly distorted square antiprism.[9] The churchite phase exhibits a layered structure and the layers consist of edge-sharing one-dimensional chains of alternating ErO_8 and PO_4 polyhedra running along the [100] direction (Figure 5a). The 1D chains in the structure are arranged in a zig-zag fashion along the [001] direction and these chains in turn are connected to one another via edge-sharing of ErO_8 polyhedra (Figure 5b). The connection of those chains leads to the formation of two-dimensional (2D) layers, which are parallel to each other in the [010] plane (Figure 5b). The structure of churchite is built by stacking these 2D layers along the b axis and with the water molecules occupying the interlayer regions (Figure 5b). The individual 2D layers are held together via formation of H-bonds between the hydrogen atoms of the water molecules present in one of the 2D layers and the oxygen atoms of the neighboring 2D layer. This results in the formation of a three-dimensional (3D) framework. The H-bonds are also formed with the oxygen atoms present within the same layer. The oxygen atom of the water molecules also forms a part of the coordination environment of the erbium atom through bonding of oxygen atom with the erbium atom.

Selected interatomic bond distances for $REPO_4 \cdot 2\ H_2O$ (RE = Gd, Dy, Er) which were refined using synchrotron data are shown in Table 2. It can be observed in Table 2, that there are 4 unique RE-O bond distances (4[2 RE-O]) in the REO_8 polyhedra. The longest RE-O bonds are due to bidentate bonding with the adjacent phosphate anions (See Table 2 and Figure 5). In the case of PO_4 tetrahedra, two distinct P-O bond distances (2[2 P-O]) were observed. The average P-O values are typical of those found in phosphate anions. Moreover, the O-P-O bond angles in

the PO_4 tetrahedra exhibit a considerable deviation from the ideal tetrahedral angle thereby indicating the distortion of the PO_4 tetrahedra (Table 2).[9] Two of the four O-P-O bond angles are considerably lower than the ideal tetrahedral angle as a result of the participation of O atoms in the bidentate bonding with the erbium atom (Table 2).[9]

Thermal analysis (TG-DSC)

In order to understand the dehydration process and to determine the total water content in the as-synthesized churchite materials, TG-DSC experiments were performed on $REPO_4 \cdot 2\ H_2O$ (RE = Gd to Yb) samples (Figure 6 and Table 4). The results show that all samples dehydrate endothermically between 210 and 230 °C (Figure 6b). The dehydration temperature increases gradually with decreasing RE ionic radius and unit cell volume. In the structure, water molecules reside in the interlayer between the 2D layers. As the RE ion radius decreases, the interlayer becomes shorter and water molecules are held more strongly between interlayers, resulting in a gradual increase in the dehydration temperature. Thus, the dehydration reaction appears to be kinetically controlled. The laboratory PXRD analysis of post TG-DSC samples show that all the churchite $REPO_4 \cdot 2\ H_2O$ phases have dehydrated and transformed to the xenotime structure (Figure 7). It should be noted that the churchite-type $GdPO_4 \cdot 2\ H_2O$ material transforms to metastable xenotime-type $GdPO_4$ upon dehydration. Thus, dehydration of churchite-type $GdPO_4 \cdot 2\ H_2O$ appears to be one of the ways to produce xenotime-type $GdPO_4$.[46] TG-DSC analysis reveal the presence of slight excess amounts of water (more than 2 moles) in $REPO_4 \cdot 2\ H_2O$ (Figure 6 and Table 4), which could be due to the presence of surface adsorbed water. Taking into account the surface adsorbed water, the chemical formulae of the as-synthesized churchite-type materials becomes $REPO_4 \cdot (2+n)\ H_2O$ where "n" indicates the surface adsorbed water. The

enthalpies of drop solution of churchite materials were calculated using the molecular weight of this corrected molecular formula.

High temperature oxide melt solution calorimetry

Churchite phosphates - $REPO_4 \cdot (2+n)\ H_2O$

The enthalpies of drop solution (ΔH_{ds}) of $REPO_4 \cdot (2+n)\ H_2O$ materials are shown in Figure 8 and Table 5. The enthalpies of formation from oxides ($\Delta H°_{f,\ ox}$) were calculated for all compounds (Table 5) from the enthalpies of drop solution of the compounds and their respective rare earth oxides (RE_2O_3),[36,41] phosphorus pentoxide (P_2O_5)[36,41] and water.[47-50] The thermochemical cycle employed to calculate the enthalpies of formation from oxides is given in Table 6.

Figure 9 shows that the enthalpy of formation from oxides of churchite compounds $REPO_4 \cdot (2+n)\ H_2O$ becomes more exothermic with increase of the ionic radius of RE^{3+} in 8-fold coordination.[51] This trend has been already observed for anhydrous $REPO_4$ compounds.[36] A comparison of the enthalpies of formation from oxides of churchites $REPO_4 \cdot (2+n)\ H_2O$ and anhydrous $REPO_4$ phosphates (Figure 9) confirms that the enthalpies of formation of $REPO_4 \cdot (2+n)\ H_2O$ compounds are always more exothermic than their corresponding anhydrous phases. Therefore, the reaction,

$$REPO_{4(s)} + (2+n)\ H_2O_{(l)} \rightarrow REPO_4 \cdot (2+n)\ H_2O_{(s)}$$

is exothermic at room temperature by 15.0 to 25.5 kJ/mol for all churchite compounds, with no obvious dependence on ionic radius (Figure 10).

Gadolinium phosphates - $GdPO_4 \cdot n\ H_2O$

Gd-phosphates adopting the monazite-, xenotime-, rhabdophane, and churchite-type structures were synthesized to determine and compare the thermodynamic stability of each structure for this element. The enthalpies of formation from oxides, $\Delta H°_{(f,ox)}$, of Gd-monazite,

Gd-xenotime, Gd-rhabdophane, and Gd-churchite, obtained at 25 °C are reported in Table 7. The enthalpies of formation of rhabdophane $GdPO_4 \cdot 0.533\ H_2O$ and churchite $GdPO_4 \cdot 2.03\ H_2O$ are -303.67 ± 1.36 kJ/mol and -318.67 ± 1.67 kJ/mol, respectively. Thus the enthalpy of formation of rhabdophane is more exothermic than that of monazite, in agreement with the data reported by Shelyug *et al*.[52] In that study, standard Gibbs free energies from oxides ($\Delta G°_{f,ox}$) of rhabdophane (-278.80 ± 6.10 kJ/mol) and monazite (-291.80 ± 1.05 kJ/mol) calculated from solubility data,[53] confirmed that rhabdophane was metastable with respect to monazite plus water. That work[52] also found that standard entropy of formation from oxides ($\Delta S°_{f,ox}$) of Gd-rhabdophane (-86.00 ± 7.20 J mol^{-1} K^{-1}), calculated by combining Gibbs free energy and enthalpy of formation at 25 °C, is more negative than that of Gd-monazite (-8.30 ± 7.60 J mol^{-1} K^{-1}) due to the confinement of liquid water in the rhabdophane structure. Thus, the metastability of Gd-rhabdophane with respect to Gd-monazite plus water is driven by the significant negative entropy associated with hydration, which is not compensated by the negative enthalpy of hydration, even at room temperature. Similarly, churchite, which has more water than rhabdophane, is likely to have entropy of formation from oxides more negative than that of rhabdophane, monazite, and xenotime. Hence, churchite ($GdPO_4 \cdot 2.03\ H_2O$) materials is also expected to be metastable with respect to rhabdophane plus water, monazite plus water, and xenotime plus water.

The enthalpy of formation of xenotime $GdPO_4$, which was formed by dehydration of churchite $GdPO_4 \cdot 2.03\ H_2O$ is -284.07 ± 0.95 kJ/mol. Since, there are no water molecules in the xenotime structure, the entropy of formation from oxides of Gd-xenotime can be assumed to be very similar to that of Gd-monazite (-8.30 ± 7.60 J mol^{-1} K^{-1}). Then, the standard Gibbs free energy of formation from oxides of Gd-xenotime is calculated to be -281.59 ± 0.95 kJ/mol. It is less negative than that of Gd-monazite (-291.80 ± 1.05 kJ/mol) reflecting the difference in

enthalpy and confirming the metastability of Gd-xenotime. Thus, Gd-monazite is the thermodynamically most stable phase followed by Gd-xenotime, Gd-rhabdophane and Gd-churchite (Figure 11 and Table 7).

The more negative enthalpies of formation for churchite $REPO_4 \cdot 2\ H_2O$ compared to anhydrous xenotime $REPO_4$[52] imply that the enthalpies of formation of churchite phases are more exothermic than those of anhydrous xenotime phases. However, the presence of water molecules in churchite $REPO_4 \cdot 2\ H_2O$ means that their entropies of formation are likely to be more negative than those for anhydrous $REPO_4$ (xenotime), which would significantly affect the Gibbs free energy of formation and stability. Thus, if churchite phases have any stability field relative to xenotime plus water, it would be limited to low temperature (probably room temperature or lower). In environmental conditions, the transformation of xenotime to churchite may be thermodynamically favorable at low temperatures. Such thermodynamic stability may explain why the precipitation of churchite materials is easier than their xenotime counterparts at lower temperatures when starting from heavy RE and phosphate ions in solution. Additionally, even if churchite is metastable, its precipitation may be kinetically favored as long as the free energies of the hydrous and anhydrous phases are similar.

Such interplay between churchite and xenotime phases may be similar to that already observed for rhabdophane and monazite.[22,28] Indeed, for light RE elements, it was found that rhabdophane was rapidly precipitated at the surface of monazite materials during leaching under weathering conditions and low temperatures. Rhabdophane precipitation then acts as a very efficient process in delaying the elemental releases in solution from the initial radwaste ceramic. Moreover, monazite materials have high chemical stability since associated normalized dissolution rates are found to be very low thereby reducing the source term in the field of an

underground repository of radioactive waste. The kinetic and thermodynamic stabilization of monazites can be proved by their common occurrence in natural assemblies and the use of such phases for geochronology (closed system over time). Thus, one could consider that the churchite-xenotime system could follow the same trend for heavy RE: the churchite precipitates as a neoformed phase on the surface of the xenotime mineral during the dissolution at lower temperatures. Therefore, the thermodynamic data of churchite obtained in this work are essential, as they contribute to the better understanding about the stability of $REPO_4$ phases in the presence of water.

Conclusions

Materials adopting the churchite structure ($REPO_4 \cdot 2\ H_2O$; RE = Gd to Lu) were synthesized and studied using PXRD and high temperature oxide melt solution calorimetry. Rietveld refinement of the synchrotron PXRD patterns of the $REPO_4 \cdot 2\ H_2O$ (RE = Gd, Dy, Er, Tb) showed that the churchite materials crystallize in the monoclinic crystal system with a layered structure similar to gypsum ($CaSO_4 \cdot 2\ H_2O$). Enthalpies of formation of the churchite materials were determined using high temperature oxide melt solution calorimetry. The enthalpies of formation from the oxides of churchite-type $REPO_4 \cdot (2+n)\ H_2O$ compounds were always found to be more exothermic than those of xenotime-type $REPO_4$ without significant dependence on the RE^{3+} ionic radius. From the obtained data, churchite materials appear of significant interest in the field of radioactive waste management. Under a failed container situation in the geological repository, the churchite materials which could form at the surface of the xenotime wasteform during aqueous alteration (including repository relevant conditions) could play an important role in delaying the release of actinides (e.g., americium and curium) to the biosphere.

ASSOCIATED CONTENT

Supporting Information.

Crystallographic files in CIF format for $ErPO_4 \cdot 2\ H_2O$, $DyPO_4 \cdot 2\ H_2O$ and $GdPO_4 \cdot 2\ H_2O$ have been deposited with the Cambridge Crystallographic Data Centre as CCDC# 1909900, CCDC# 1909899, CCDC# 1909901. These data may be obtained free of charge by contacting CCDC at (https://www.ccdc.cam.ac.uk/).

AUTHOR INFORMATION

Corresponding Author

*E-mail: adel.mesbah@cea.fr (A. M.)

*E-mail: anavrotsky@ucdavis.edu (A. N.)

ACKNOWLEDGMENT

The calorimetric studies at UC Davis were supported by the U.S. Department of Energy grant DE-FG02-03ER46053. The work in France also benefited from financial support of the French National Research Agency (ANR JCJC-X-MAS^2; project # ANR-17-CE06-0004).

Figures

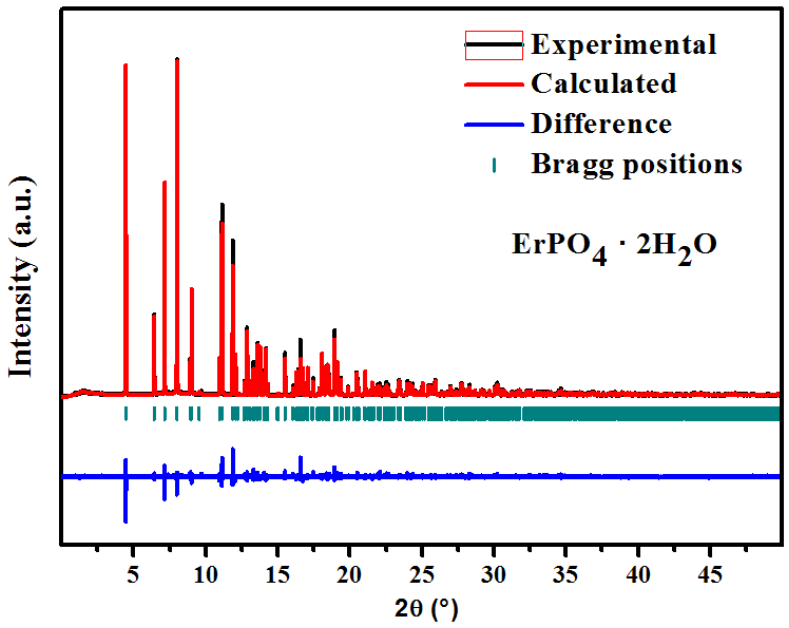

Figure 1. Rietveld refined synchrotron powder XRD pattern of churchite-type $ErPO_4 \cdot 2\ H_2O$ material

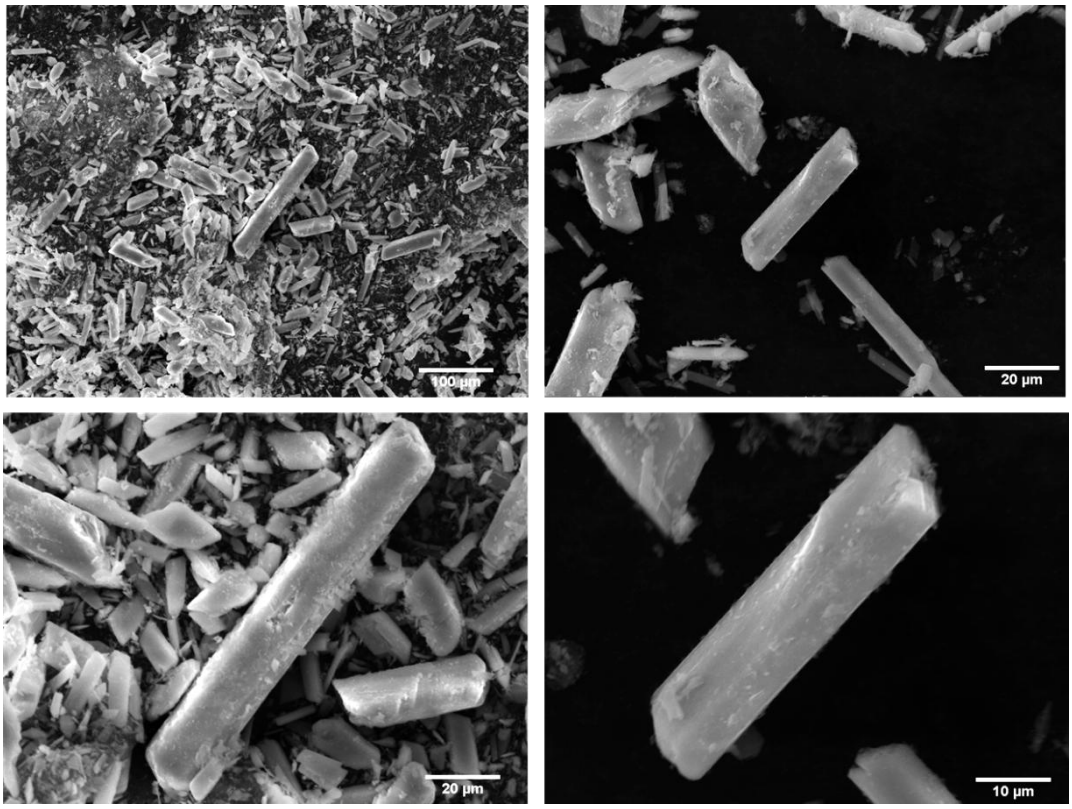

Figure 2. SEM micrographs of Churchite-type $ErPO_4 \cdot 2\ H_2O$ material

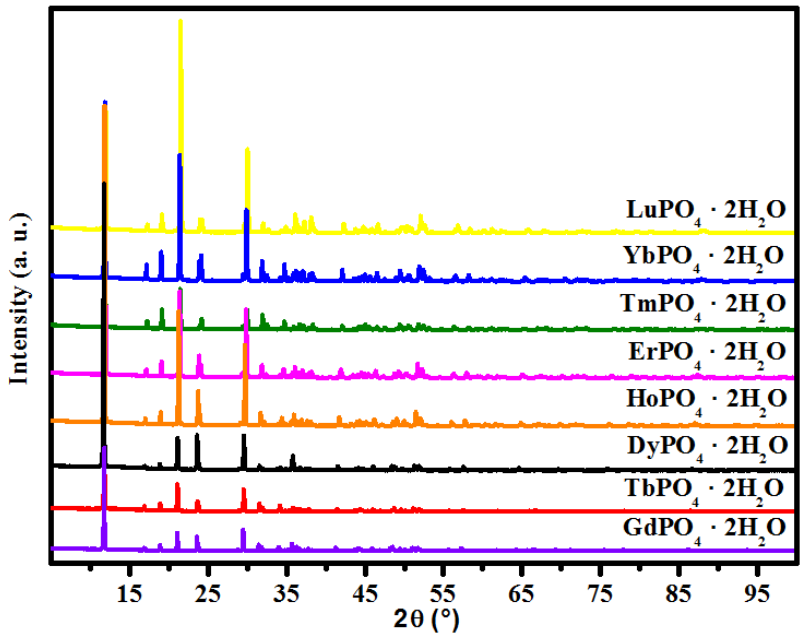

Figure 3. Laboratory powder XRD patterns of the churchite-type $REPO_4 \cdot 2\ H_2O$ (RE = Gd to Lu) materials

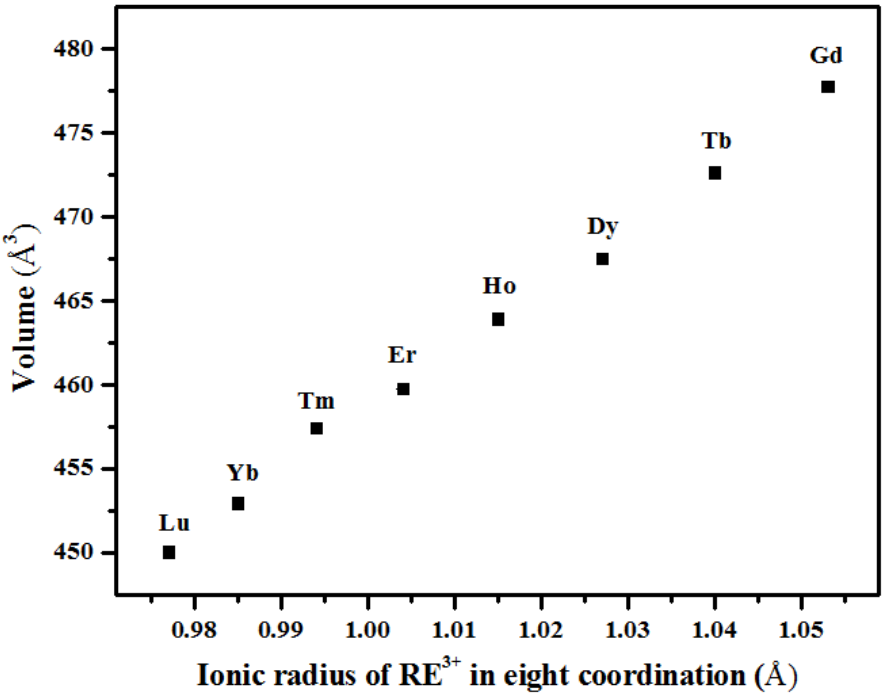

Figure 4. Evolution of the refined unit cell volume in the $REPO_4 \cdot 2\ H_2O$ based compounds with RE = Gd to Lu

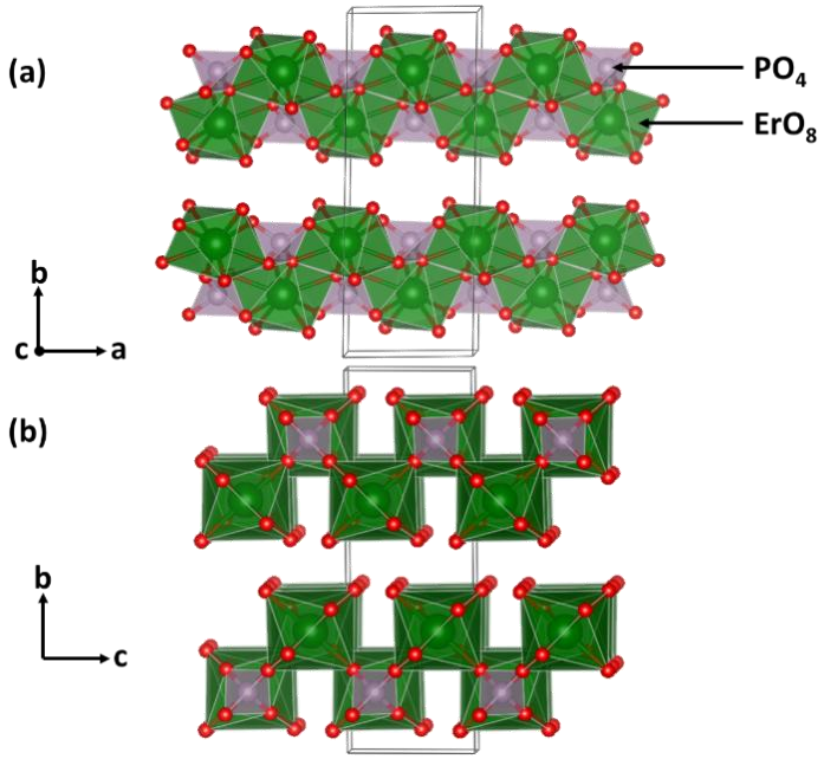

Figure 5. Crystal structure of churchite-type $ErPO_4 \cdot 2\ H_2O$ (Space group: *C2/c*) oriented along the (a) 'c' and (b) 'a' direction. The crystal structures were generated using the VESTA program.[45]

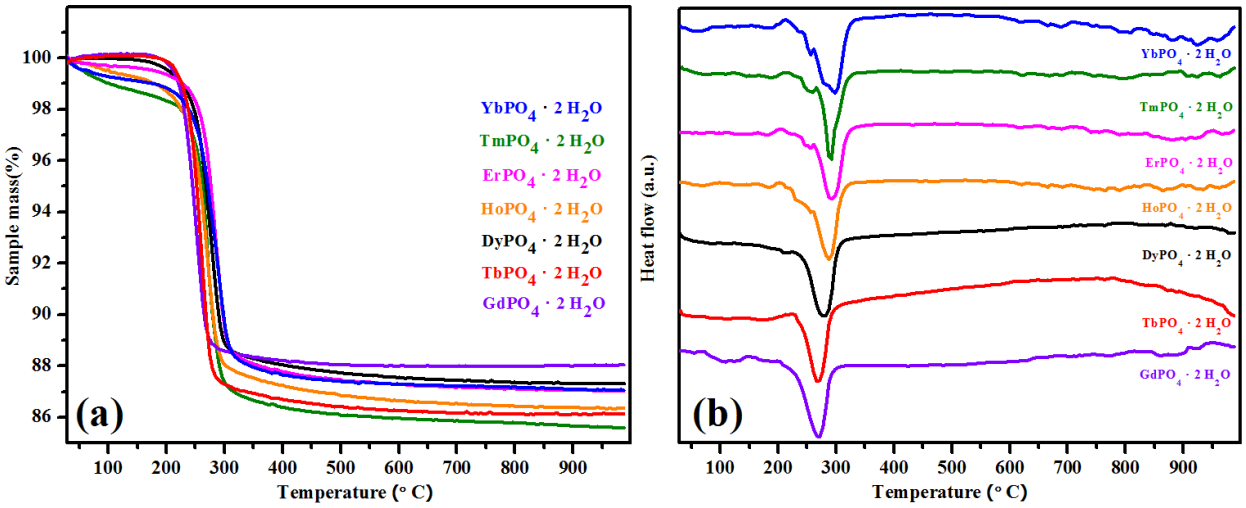

Figure 6. TG (a) and DSC (b) scans of churchite-type $REPO_4 \cdot 2\ H_2O$ (RE = Gd to Yb)

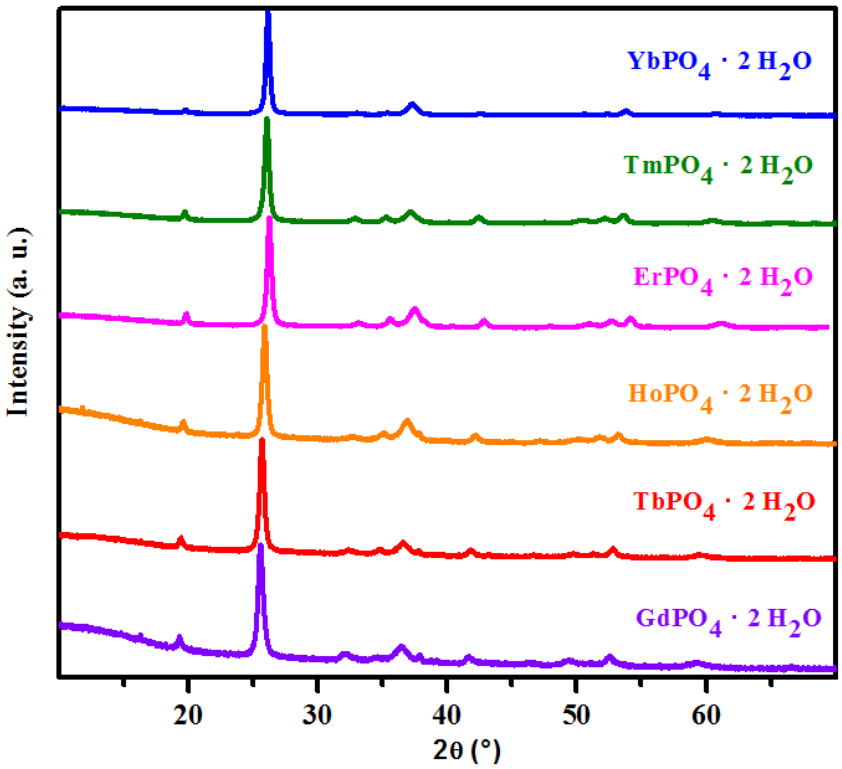

Figure 7. PXRD patterns of the churchite-type $REPO_4 \cdot 2\ H_2O$ after TG-DSC at 1000°C showing the formation of xenotime-type $REPO_4$ on dehydration

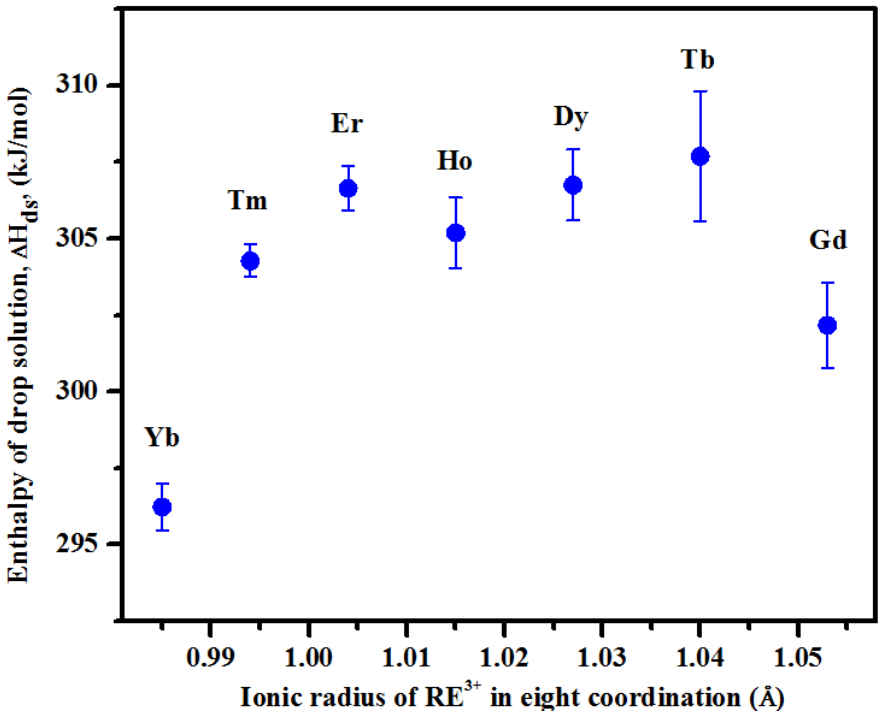

Figure 8. Enthalpies of drop solution (ΔH_{ds}) of $REPO_4 \cdot (2+n)\ H_2O$ vs ionic radius of RE^{3+}

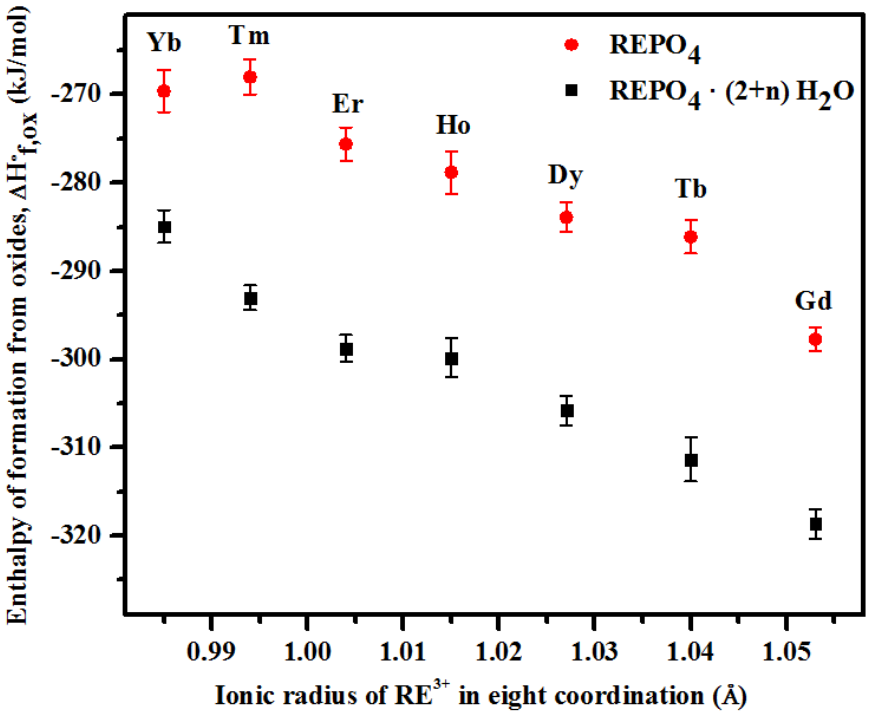

Figure 9. Enthalpies of formation from oxides ($\Delta H^\circ_{(f,\,ox)}$) of $REPO_4$ and $REPO_4 \cdot (2+n)\ H_2O$ vs ionic radius of RE^{3+}. Data for $REPO_4$ is taken from Ref. 36.

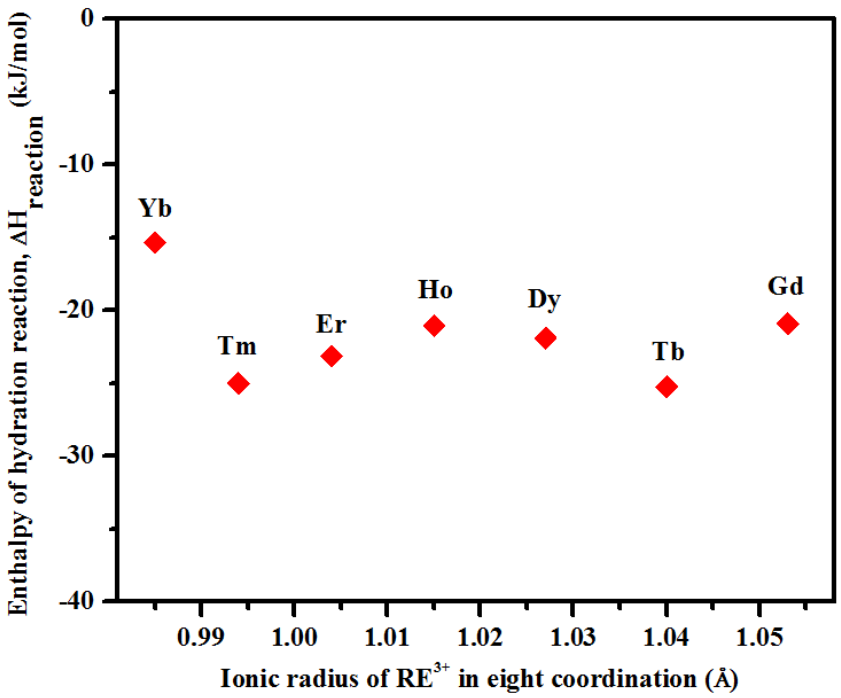

Figure 10. Enthalpies of hydration reaction $REPO_{4(s)} + (2+n)\ H_2O_{(l)} \rightarrow REPO_4 \cdot (2+n)\ H_2O_{(s)}$ vs Ionic radius of RE^{3+}

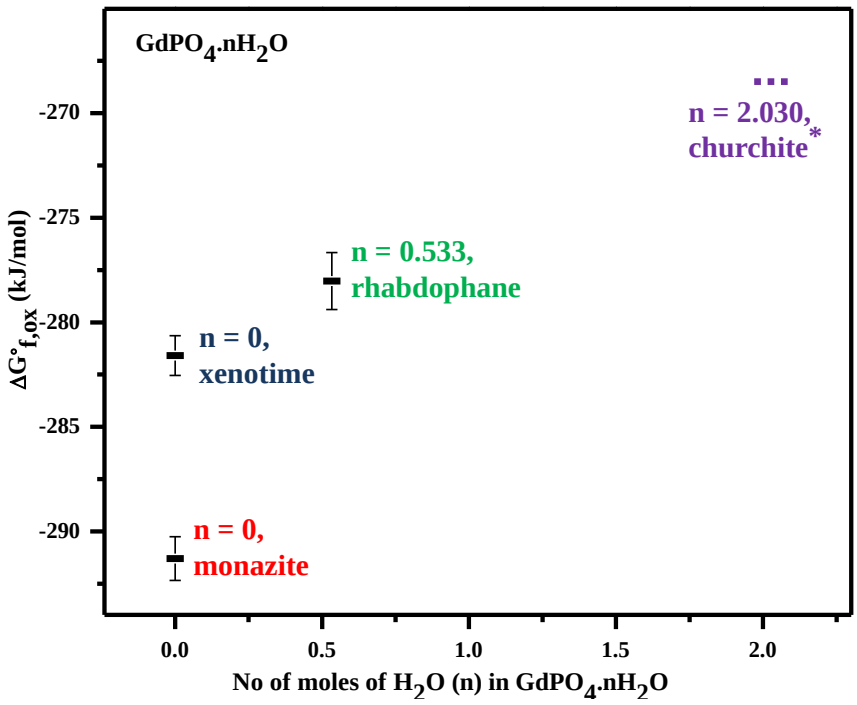

Figure 11. Standard Gibbs free energy of formation from oxides ($\Delta G°_{f,ox}$) obtained for $GdPO_4 \cdot n\ H_2O$ versus the number of water molecules, n, in $GdPO_4 \cdot n\ H_2O$ (*$\Delta G°_{f,ox}$ of churchite phase when $\Delta S°_{f,ox}$ is considered twice that of rhabdophane phase)

Tables

Table 1. Crystallographic data and Structure Refinement of $REPO_4 \cdot 2\ H_2O$ (RE = Er, Dy, Gd)

Sample	**$ErPO_4 \cdot 2\ H_2O$**	**$DyPO_4 \cdot 2\ H_2O$**	**$GdPO_4 \cdot 2\ H_2O$**
Formula weight (g/mol)	298.26	293.50	288.25
T (°C)	25	25	25
Crystal System	Monoclinic	Monoclinic	Monoclinic
Space group	*C* 2/*c*	*C* 2/*c*	*C* 2/*c*
a	6.1527(1)	6.1889(1)	6.2359(1)
b	15.0177 (1)	15.0797(1)	15.1777(1)
c	5.5857(1)	5.6106(1)	5.6409(1)
B	115.47 (1)	115.22(1)	114.95(1)
V ($Å^3$)	465.94 (1)	473.71 (1)	484.07(1)
Z	4	4	4
Wavelength (Å)	0.58403	0.58403	0.58403
R_p	0.099	0.104	0.095
R_{wp}	0.127	0.137	0.122
R_{Bragg}	0.072	0.062	0.046
R_F	0.073	0.057	0.044

Table 2. Selected interatomic bond distances (Å) and bond angles (°) of $REPO_4 \cdot 2\ H_2O$ (RE = Er, Dy, Gd)

	$ErPO_4 \cdot 2\ H_2O$	**$DyPO_4 \cdot 2\ H_2O$**	**$GdPO_4 \cdot 2\ H_2O$**
Bond distance (Å)			
(Ln-O1) × 2	2.439 (4)	2.458(6)	2.480(4)
(Ln-O2) × 2	2.453 (4)	2.465(5)	2.491(3)
(Ln-O2) × 2	2.289 (5)	2.311(5)	2.333(3)
(Ln-O3) × 2	2.397 (5)	2.409(4)	2.431(3)
(P-O1) × 2	1.557 (4)	1.550(4)	1.543(3)
(P-O2) × 2	1.527 (4)	1.525(6)	1.536(4)
Bond angle (°)			
O1-P-O2	103.7 (2)	103.7(5)	111.2(4)
O1-P-O2	112.9(5)	111.2(5)	103.9(3)
O1-P1-O1	113.2 (3)	114.7(4)	114.1(3)
O2-P-O2	110.6 (4)	112.7(6)	112.9(5)

Table 3. Lattice constants of $REPO_4 \cdot 2\ H_2O$ (RE = Gd - Lu)

Sample	a (Å)	b (Å)	c (Å)	β (°)	V (Å^3)
$GdPO_4 \cdot 2\ H_2O$	6.2103 (1)	15.1105 (24)	5.6163 (1)	114.96 (1)	477.82(1)
$TbPO_4 \cdot 2\ H_2O$	6.1868 (1)	15.0437 (3)	5.6071 (1)	115.08 (1)	472.67(2)
$DyPO_4 \cdot 2\ H_2O$	6.1671 (7)	15.0123 (5)	5.5844 (4)	115.26 (8)	467.58(6)
$HoPO_4 \cdot 2\ H_2O$	6.1466 (2)	14.9854 (3)	5.5743 (2)	115.36 (2)	463.96(2)
$ErPO_4 \cdot 2\ H_2O$	6.1265 (2)	14.9509 (3)	5.5602 (2)	115.47 (2)	459.79(2)
$TmPO_4 \cdot 2\ H_2O$	6.1175 (8)	14.9114 (2)	5.5588 (8)	115.56 (6)	457.46(1)
$YbPO_4 \cdot 2\ H_2O$	6.1000 (8)	14.8712 (2)	5.5401 (9)	115.66 (8)	453.00(1)
$LuPO_4 \cdot 2\ H_2O$	6.0879 (2)	14.8546 (5)	5.5289 (2)	115.82 (2)	450.08(2)

Table 4 Summary of weight loss measurements from TG-DSC studies

Sample	Number of H_2O molecules corresponding to weight loss	Number of excess (surface adsorbed) H_2O molecules 'n'
$GdPO_4 \cdot 2\ H_2O$	2.03	0.03
$TbPO_4 \cdot 2\ H_2O$	2.05	0.05
$DyPO_4 \cdot 2\ H_2O$	2.04	0.04
$HoPO_4 \cdot 2\ H_2O$	2.08	0.08
$ErPO_4 \cdot 2\ H_2O$	2.07	0.07
$TmPO_4 \cdot 2\ H_2O$	2.06	0.06
$YbPO_4 \cdot 2\ H_2O$	2.07	0.07

Table 5. Enthalpies of drop solution (ΔH_{ds}) of churchite $REPO_4 \cdot 2\ H_2O$ in $3\ Na_2O \cdot 4\ MoO_3$ solvent at 700 °C and enthalpies of formation from oxides ($\Delta H°_{f,ox}$)

Sample	ΔH_{ds} (kJ/mol)	$\Delta H°_{(f,\ ox)}$ (kJ/mol)
$GdPO_4 \cdot 2.03\ H_2O$	302.17 ± 1.39 (8)[a]	-318.67 ± 1.67
$TbPO_4 \cdot 2.05\ H_2O$	307.69 ± 2.14 (7)	-311.33 ± 2.50
$DyPO_4 \cdot 2.04\ H_2O$	306.81 ± 1.16 (9)	-305.79 ± 1.67
$HoPO_4 \cdot 2.08\ H_2O$	305.19 ± 1.15 (9)	-299.83 ± 2.22
$ErPO_4 \cdot 2.07\ H_2O$	306.64 ± 0.74 (8)	-298.74 ± 1.52
$TmPO_4 \cdot 2.06\ H_2O$	304.27 ± 0.53 (8)	-292.99 ± 1.39
$YbPO_4 \cdot 2.07\ H_2O$	296.23 ± 0.75 (7)	-284.93 ± 1.82

[a]Error is two standard deviations of the mean and number in () is number of individual experiments performed.

Table 6. Thermochemical cycle for the calculation of enthalpy of formation from oxides for $REPO_4.(2+n)\ H_2O$ churchite phase

Reaction		**ΔH (kJ/mol)**
$REPO_4 \cdot (2 + n)\ H_2O_{(s,25)} \rightarrow$ ½ $RE_2O_{3(sln,700)}$ + ½ $P_2O_{5(sln,700)}$ + (2 + n) $H_2O_{(g,700)}$	[1]	$\Delta H_{ds}(REPO_4 \cdot (2+n)\ H_2O)$ [Table 5]
$RE_2O_{3(s,25)} \rightarrow RE_2O_{3(sln,700)}$	[2]	$\Delta H_{ds}(RE_2O_3)$[36, 41]
$P_2O_{5(s,25)} \rightarrow P_2O_{5(sln,700)}$	[3]	$\Delta H_{ds}(P_2O_5)$=-164.60±0.85[36]
$H_2O_{(l,25)} \rightarrow H_2O_{(g,700)}$	[4]	$\Delta H(H_2O)$=69.00± 0.10[47-50]
½ $RE_2O_{3(s,25)}$ + ½ $P_2O_{5(s,25)}$ + (2+n) $H_2O_{(l,25)} \rightarrow$ $REPO_4 \cdot (2 + n)\ H_2O_{(s,25)}$	[5]	$\Delta H°_{f,ox}(REPO_4 \cdot (2+n)\ H_2O)$ [Table 5]
$\Delta H[5] = -\Delta H[1] + ½\ \Delta H[2] + ½\ \Delta H[3] + (2 + n)\ \Delta H[4]$		

Table 7 Enthalpies of drop solution (ΔH_{ds}) in 3 $Na_2O \cdot 4\ MoO_3$ solvent at 700 °C and associated enthalpies, entropies and free Gibbs energies of formation from oxides, $\Delta H°_{f,ox}$, $\Delta S°_{f,ox}$ and $\Delta G°_{f,ox}$ obtained for Gd-xenotime, Gd-monazite, Gd-rhabdophane and Gd-churchite. $\Delta G°_{f,ox}$ values were calculated at 298.15 K (25 °C)

Sample	**Number of water molecules 'n'**	**ΔH_{ds} (kJ/mol)[a]**	**$\Delta H°_{f,ox}$ (kJ/mol)[b]**	**$\Delta S°_{f,ox}$ (J mol^{-1} K^{-1})[c]**	**$\Delta G°_{f,ox}$ (kJ/mol)**
$GdPO_4$ – xenotime	0	127.47±0.29 (4)	-284.07±0.95	-8.30±7.60	-281.59±0.95
$GdPO_4$ – monazite	0	137.71±0.53 (7)	-294.28±1.05	-8.30±7.60	-291.80±1.05
$GdPO_4 \cdot 0.533\ H_2O$ – rhabdophane	0.533	183.88±0.83 (8)	-303.67±1.36	-86.00±7.20	-278.03±1.36
$GdPO_4 \cdot 2.03\ H_2O$ – churchite	2.030	302.17±1.39 (8)	-318.67±1.67	-	-

[a]Error is two standard deviations of the mean and number in () is number of individual experiments performed.
[b]Determined in this study
[c]Determined by Shelyug *et al*(Ref. 52)

REFERENCES

(1) Ewing, R. C.; Wang, L. Phosphates as Nuclear Waste Forms. *Rev. Mineral. Geochem.* **2002**, 48, 673–699.

(2) Oelkers, E. H.; Montel, J-M. Phosphates and Nuclear Waste Storage. *Elements* **2008**, 4, 113–116.

(3) Montel, J-M. Minerals and design of new waste forms for conditioning nuclear waste. *C R Geosci.* **2011**, 343, 230–236.

(4) Achary, S. N.; Bevara, S.; Tyagi, A. K. Recent progress on synthesis and structural aspects of rare-earth phosphates. *Coord. Chem. Rev.* **2017**, 340, 266–297.

(5) Rafiuddin, M. R.; Grosvenor, A. P. A Structural Investigation of Hydrous and Anhydrous Rare-Earth Phosphates. *Inorg. Chem.* **2016**, 55, 9685–9695.

(6) Clavier, N.; Mesbah, A.; Szenknect, S.; Dacheux, N. Monazite, rhabdophane, xenotime & churchite: Vibrational spectroscopy of gadolinium phosphate polymorphs. *Spectrochim. Acta Part A Mol. Biomol. Spectrosc.* **2018**, 205, 85–94.

(7) Ni, Y.; Hughes, J. M.; Mariano, A. N. Crystal chemistry of the monazite and xenotime structures. *Am. Mineral.* **1995**, 80, 21–26.

(8) Mesbah, A.; Clavier, N.; Elkaim, E.; Gausse, C.; Ben Kacem, I.; Szenknect, S.; Dacheux, N. Monoclinic form of the rhabdophane compounds: $REEPO_4.0.667H_2O$. *Cryst. Growth Des.* **2014**, 14, 5090–5098.

(9) Ivashkevich, L. S.; Lyakhov, A. S.; Selevich, A. F. Preparation and structure of the yttrium phosphate dihydrate. *Phosphorus Res. Bull.* **2013**, 28, 45–50.

(10) Kohlmann, M.; Sowa, H.; Reithmayer, K.; Schulz, H.; Krüger, R. R.; Abriel, W. Structure of a $Y_{1-x}(Gd,Dy,Er)_xPO_4.2H_2O$ microcrystal using synchrotron radiation. *Acta Crystallogr. Sect. C Cryst. Struct. Commun.* **1994**, 50, 1651–1652.

(11) Zepf, V. *Rare Earth Elements: What and Where They Are. In: Rare Earth Elements Springer Theses (Recognizing Outstanding Ph.D. Research)*; Springer: Berlin, 2013; Heidelberg

(12) Voncken, J. H. L. *The Ore Minerals and Major Ore Deposits of the Rare Earths, in: The Rare Earth Elements*; SpringerBriefs in Earth Sciences. Springer: Cham, 2016.

(13) Emden, B.; Thornber, M. R.; Graham, J.; Lincoln, F. J. The incorporation of actinides in monazite and xenotime from placer deposits in Western Australia. *Can. Mineral.* **1997**, 35, 95-104.

(14) Spear, F. S.; Pyle, J. M. Apatite, Monazite, and Xenotime in Metamorphic Rocks. *Rev. Mineral. Geochemistry.* **2002**, 48, 293-335.

(15) Karioris, F. G.; Gowda, K. A.; Cartz, L. Heavy ion bombardment of monoclinic $ThSiO_4$, ThO_2 and Monazite. *Radiat. Eff. Lett.* **1981**, 58, 1–3.

(16) Meldrum, A.; Boatner, L. A.; Weber, W. J.; Ewing, R. C. Radiation damage in zircon and monazite. *Geochim. Cosmochim. Acta.***1998**, 62, 2509–2520.

(17) Rafiuddin, M. R.; Grosvenor, A. P. Probing the effect of radiation damage on the structure of rare-earth phosphates. *J. Alloys Compd.* **2015**, 653, 279–289.

(18) Lu, F.; Shen, Y.; Sun, X.; Dong, Z.; Ewing, R. C., Lian, J. Size dependence of radiation-induced amorphization and recrystallization of synthetic nanostructured $CePO_4$ monazite.

Acta Mater. **2013**, 61, 2984–2992.

(19) Meldrum, A.; Boatner, L.; Ewing, R. Displacive radiation effects in the monazite- and zircon-structure orthophosphates. *Phys. Rev. B.* **1997**, 56, 13805–13814.

(20) Seydoux-Guillaume, A-M.; Deschanels, X.; Baumier, C.; Neumeier, S.; Weber, W. J.; Peuget, S. Why natural monazite never becomes amorphous: Experimental evidence for alpha self-healing. *Am. Mineral.* **2018**, 103, 824-827.

(21) Gausse, C.; Szenknect, S.; Mesbah, A.; Clavier, N.; Neumeier, S.; Dacheux, N. Dissolution kinetics of monazite $LnPO_4$ (Ln = La to Gd): A multiparametric study. *Appl. Geochem.* **2018**, 93, 81–93.

(22) Dacheux, N.; Clavier, N.; Podor, R. Monazite as a promising long-term radioactive waste matrix: Benefits of high-structural flexibility and chemical durability. *Am. Mineral.* **2013**, 98, 833–847.

(23) Arinicheva, Y.; Neumeier, S.; Brandt, F.; Bosbach, D.; Deissmann, G. Dissolution kinetics of synthetic $LaPO_4$-monazite in acidic media. *MRS Adv.* **2018**, 3, 1133–1137.

(24) Rafiuddin, M. R.; Grosvenor, A. P. An investigation of the chemical durability of hydrous and anhydrous rare-earth phosphates. *J. Nucl. Mater.* **2018**, 509, 631-643.

(25) Arinicheva, Y.; Gausse, C.; Neumeier, S.; Brandt, F.; Rozov, K.; Szenknect, S.; Dacheux, N.; Bosbach, D.; Deissmann, G. Influence of temperature on the dissolution kinetics of synthetic $LaPO_4$-monazite in acidic media between 50 and 130 °C. *J. Nucl. Mater.* **2018**, 509, 488-495.

(26) Vance, E. R.; Zhang, Y.; McLeod, T.; Davis, J. Actinide valences in xenotime and

monazite. *J. Nucl. Mater.* **2011**, 409, 221–224.

(27) Berger, A.; Gnos, E.; Janots, E.; Fernandez, A.; Giese, J. Formation and composition of rhabdophane, bastnäsite and hydrated thorium minerals during alteration: Implications for geochronology and low-temperature processes. *Chem. Geol.* **2008**, 254, 238–248.

(28) Du Fou de Kerdaniel, E.; Clavier, N.; Dacheux, N.; Terra, O.; Podor, R. Actinide solubility-controlling phases during the dissolution of phosphate ceramics. *J. Nucl. Mater.* **2007**, 362, 451–458.

(29) Li, H.; Zhu, G.; Ren, H.; Li, Y.; Hewitt, I. J.; Qiu, S. The Synthesis of Multiwalled Rare-Earth Phosphate Nanomaterials Using Organophosphates with Upconversion Properties. *Eur. J. Inorg. Chem.* **2008**, 2008, 2033–2037.

(30) Wang, L.; He, D.; Feng, S.; Yu, C.; Hu, L.; Qiu, J.; Chen, D. Phosphate ytterbium-doped single-mode all-solid photonic crystal fiber with output power of 13.8 W. *Sci. Rep.* **2015**, 5, 8490, 1-4.

(31) Kitamura, N.; Amezawa, K.; Tomii, Y.; Yamamoto, N. Protonic conduction in rare earth orthophosphates with the monazite structure. *Solid State Ionics* **2003**, 162–163, 161–165.

(32) Onoda, H.; Nariai, H.; Moriwaki, A.; Maki, H.; Motooka, I. Formation and catalytic characterization of various rare earth phosphates. *J. Mater. Chem.* **2002**, 12, 1754–1760.

(33) Meiser, F.; Cortez, C.; Caruso, F. Biofunctionalization of Fluorescent Rare-Earth-Doped Lanthanum Phosphate Colloidal Nanoparticles. *Angew. Chemie Int. Ed.* **2004**, 43, 5954–5957.

(34) Mesbah, A.; Clavier, N.; Elkaim, E.; Szenknect, S.; Dacheux, N. In pursuit of the

rhabdophane crystal structure: from the hydrated monoclinic $LnPO_4.0.667H_2O$ to the hexagonal $LnPO_4$ (Ln = Nd, Sm, Gd, Eu and Dy). *J. Solid State Chem.* **2017**, 249, 221–227.

(35) Assaaoudi, H.; Ennaciri, A.; Rulmont, A.; Harcharras, M. Gadolinium orthophosphate weinschenkite type and phase change in rare earth orthophosphates, *Phase Transitions*. **2000**, 72, 1–13.

(36) Ushakov, S. V.; Helean, K. B.; Navrotsky, A.; Boatner, L. A. Thermochemistry of rare-earth orthophosphates. *J. Mater. Res.* **2001**, 16, 2623–2633.

(37) Hirsch, A.; Kegler, P.; Alencar, I.; Ruiz-Fuertes, J.; Shelyug, A.; Peters, L.; Schreinemachers, C.; Neumann, A.; Neumeier, S.; Liermann, H.-P.; Navrotsky, A.; Roth, G.; Structural, vibrational, and thermochemical properties of the monazite-type solid solution $La_{1-x}Pr_xPO_4$. *J. Solid State Chem.* **2017**, 245, 82–88.

(38) Neumeier, S.; Kegler, P.; Arinicheva, Y.; Shelyug, A.; Kowalski, P. M.; Schreinemachers, C.; Navrotsky, A.; Bosbach, D.; Thermochemistry of $La_{1-x}Ln_xPO_4$-monazites (Ln=Gd, Eu). *J. Chem. Thermodyn.* **2017**, 105, 396–403.

(39) Dinnebier, R.; *Rietveld Refinement from Powder Diffraction Data*, 2001.

(40) Finger, L. W.; Cox, D. E.; Jephcoat, A. P.; Correction for powder diffraction peak asymmetry due to axial divergence *J. Appl. Crystallogr.***1994**, *27*, 892–900.

(41) Navrotsky, A. Progress and New Directions in Calorimetry: A 2014 Perspective. *J. Am. Ceram. Soc.* **2014**, 97, 3349–3359.

(42) Navrotsky, A. Mineralogy, materials science, energy, and environment: A 2015 perspective. *Am. Mineral.* **2015**, 100, 674–680.

(43) Navrotsky, A. Progress and new directions in high temperature calorimetry. *Phys. Chem. Miner.* **1977**, 2, 89–104.

(44) Navrotsky, A. Progress and new directions in high temperature calorimetry revisited. *Phys. Chem. Miner.* **1997**, 24, 222–241.

(45) Momma, K.; Izumi, F. VESTA: a three-dimensional visualization system for electronic and structural analysis. *J. Appl. Crystallogr.* **2008**, 41, 653–658.

(46) Rodriguez-Liviano, S.; Becerro, A. I.; Alcantara, D.; Grazu, V.; de la Fuente, J. M.; Ocana, M. Synthesis and properties of multifunctional tetragonal Eu:$GdPO_4$ nanocubes for optical and magnetic resonance imaging applications. *Inorg. Chem.* **2013**, 52, 647–654.

(47) Maloney, J. O. *Perry's Chemical Engineers Handbook 8th Edition - Section 1, 8th Edition*; McGraw-Hill: New York, 2008.

(48) Barin, I. *Thermochemical Data of Pure Substances*; VCH: Weinheim, 1995.

(49) Chase, M. W.; Davies, C. A.; Frurip, D. J.; McDonald, R. A.; Syverud, A. N.; *NIST-JANAF Thermochemical Tables, Third Edition*; The American Chemical Society and the American Institute of Physics for the National Institute of Standards and Technology: Gaithersburg, 1985.

(50) Bale, C.; Bélisle, E.; Chartrand, P.; Decterov, S.; Eriksson, G.; Gheribi, A.; Hack, K.; Jung, I.-H.; Kang, Y.- B.; Melançon, J.; Pelton, A.; Petersen, S.; Robelin, C.; Sangster,

J; Spencer, P.; VanEnde, M.-A. FactSage thermochemical software and databases, 2010–2016. *CALPHAD: Comput. Coupling Phase Diagrams Thermochem.* **2016**, 54, 35–53. doi: 10.1016/j.calphad.2016.05.002.

(51) Shannon, R. D. Revised effective ionic radii and systematic studies of interatomic distances in halides and chalcogenides, *Acta Crystallogr. Sect. A.* **1976**, 32, 751–767. doi:10.1107/S0567739476001551.

(52) Shelyug, A.; Mesbah, A.; Szenknect, S.; Clavier, N.; Dacheux, N.; Navrotsky, A. Thermodynamics and stability of rhabdophanes, hydrated rare earth phosphates $REPO_4.n\ H_2O$. *Front. Chem.* **2018**, 6, 604. doi: 10.3389/fchem.2018.00604

(53) Gausse, C.; Szenknect, S.; Qin, D. W.; Mesbah, A.; Clavier, N.; Neumeier, S.; Bosbach, D.; Dacheux, N. Determination of the Solubility of Rhabdophanes $LnPO_4.0.667H_2O$ (Ln = La to Dy). *Eur. J. Inorg. Chem.* **2016**, 28, 4615–4630.

FOR TABLE OF CONTENTS USE ONLY

Authors: Tamilarasan Subramani, Mohamed Ruwaid Rafiuddin, Anna Shelyug, Sergey Ushakov, Adel Mesbah, Nicolas Clavier, Danwen Qin, Stephanie Szenknect, Erik Elkaim,, Nicolas Dacheux, Alexandra Navrotsky

Synopsis:

Churchite-type materials ($REPO_4 \cdot 2H_2O$; RE = Gd to Yb) adopt the gypsum structure and were synthesized using a precipitation route. The enthalpies of formation from oxides ($\Delta H_{f,ox}$) of churchite were determined using high temperature oxide melt solution calorimetry. The $\Delta H_{f,ox}$ of churchite materials was more exothermic than their anhydrous counterparts adopting the xenotime structure. The Gibbs free energy of formation from oxides ($\Delta G°_{f,ox}$) of Gd-phosphates data suggests that the Gd-monazite is the thermodynamically stable phase.